ACS APPLIED MATERIALS & INTERFACES

Research Article

www.acsami.org

Magnetic Alignment of Hexagonal Boron Nitride Platelets in Polymer Matrix: Toward High Performance Anisotropic Polymer Composites for Electronic Encapsulation

Ziyin Lin,[†] Yan Liu,[†] Sathyanarayanan Raghavan,[‡] Kyoung-sik Moon,[†] Suresh K. Sitaraman,[†] and Ching-ping Wong*[,†,§]

[†]School of Materials Science and Engineering, [‡]School of Mechanical Engineering Georgia Institute of Technology, 771 Ferst Drive, Atlanta, Georgia 30332, United States

[§]Department of Electronic Engineering, The Chinese University of Hong Kong, Hong Kong

Supporting Information

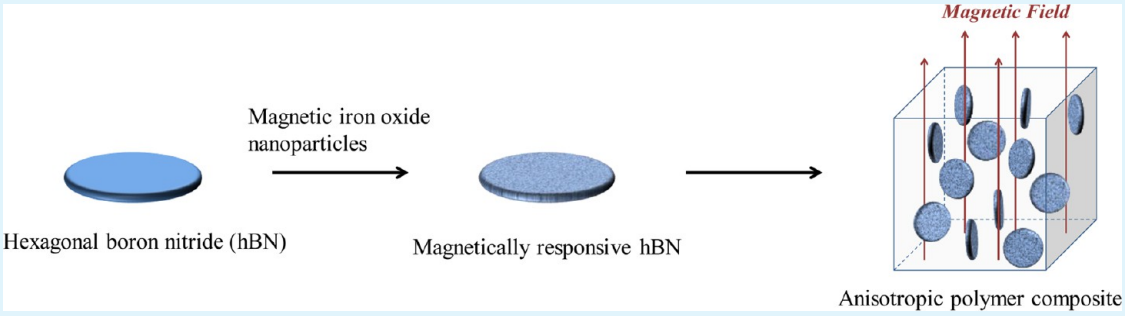

ABSTRACT: We report magnetic alignment of hexagonal boron nitride (hBN) platelets and the outstanding material properties of its polymer composite. The magnetically responsive hBN is produced by surface modification of iron oxide, and their orientations can be controlled by applying an external magnetic field during polymer curing. Owing to the anisotropic properties of hBN, the epoxy composite with aligned hBN platelets shows interesting properties along the alignment direction, including significantly reduced coefficient of thermal expansion, reaching ~28.7 ppm/°C, and enhanced thermal conductivity, 104% higher than that of unaligned counterpart, both of which are observed at a low filler loading of 20 wt %. Our modeling suggests the filler alignment is the major reason for these intriguing material properties. Finite element analysis reveals promising applications for the magnetically aligned hBN-based composites in modern microelectronic packaging.

KEYWORDS: *hexagonal boron nitride, polymer composite, magnetic alignment, thermal conductivity, coefficient of thermal expansion*

1. INTRODUCTION

The rapid development of new generation electronics, fine-pitch integrated circuits (ICs) and three-dimensional (3D) integration set stringent requirements for packaging materials to ensure the long lifetime of electronic devices.[1−3] High thermal conductivity, electrical insulating, and low coefficient of thermal expansion (CTE) polymer composites are in great need as encapsulants for ICs to provide environmental protection, facilitate the heat dissipation, and relieve the thermal stress. Conventional underfill materials, containing polymers and silica fillers, are widely used in current electronics but cannot meet these requirements due to their poor thermal conductivity of lower than 0.5 W/mK that results from the low intrinsic thermal conductivity of silica fillers (1.4 W/mK). Thermal interface materials (TIMs), another important example of polymer composite, are filled with high thermal conductivity ceramic or metallic fillers and have thermal conductivity of 1−5 W/mK. However, to reach high thermal conductivity, extremely high filler loading is required (>50 vol %), resulting in the loss of processablity and degradation of mechanical properties.[4−6] So far, the lack of high performance materials for IC encapsulation has been one of major bottlenecks for next-generation electronics.

The unsatisfactory performance of known polymer composites in electronic packaging is largely due to the slowly developed filler technology. With the excellent mechanical and adhesive properties of polymers, fillers are added to introduce desired properties for target applications: silica is used to lower the CTE for underfills because of its low CTE of 0.5 ppm/K;[7,8] high thermal conductivity ceramics are used in TIMs to improve the thermal conductivity;[5,6,9−12] and metallic fillers (silver, copper etc.) are used in electrical conductive adhesives (ECAs) to boost the electrical conductivity.[3,13] In addition to the intrinsic properties of fillers, the performances of composites are also affected by filler geometries,[12,14] orientations,[9] and interfacial properties,[7,8,15] which are being

Received: May 22, 2013
Accepted: July 1, 2013
Published: July 1, 2013

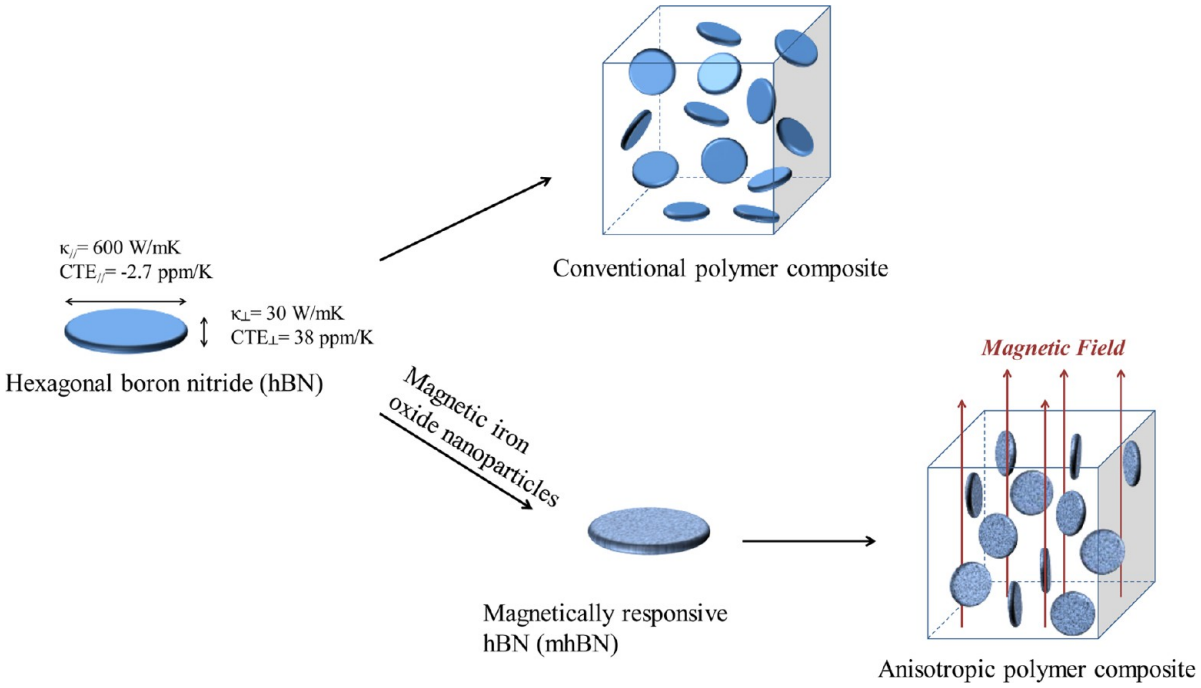

Figure 1. Anisotropic properties of hBN platelets and schematics of conventional polymer composite in which hBN platelets are randomly oriented; schematic illustration of the preparation of magnetically responsive hBN and its alignment hBN under an external magnetic field for anisotropic polymer composite.

actively researched. Among these factors, the filler alignment is less explored because of technical difficulties in controlling the filler alignment. Several approaches were used to prepare polymer composites with aligned fillers. Prealigned fillers (e.g., carbon nanotube arrays) were used to prepare the polymer composites with enhanced performance in alignment direction.[16−19] Shear alignment is another approach in which fillers are aligned by the shear force during the flow or stretch of polymers.[9,20−24] Moreover, the gravitational force can lead to horizontal alignment of high aspect ratio fillers.[25,26] However, these methods only produce composite materials with predefined geometry and filler alignment direction and therefore have limited applications. It is highly desirable to develop new methods for effective filler alignment after the application of composite and with flexible control over the alignment direction.

Magnetic alignment is very attractive in this regard due to the remote control of filler alignment and possibility of orienting filler at arbitrary directions.[27,28] A variety of structures can be achieved under optimized conditions.[28−34] In this work, we explored the magnetic alignment of hexagonal boron nitride (hBN) platelets in epoxy composites and the resulting materials properties. hBN platelets is an outstanding filler to demonstrate the impact of filler alignment not only because of its nonspherical shape but also because of its anisotropic properties. As seen in Figure 1, hBN platelets have excellent in-plane properties including high thermal conductivity of ∼600 W/mK and low CTE of −2.7 ppm/K. However, the inferior out-of-plane properties, low thermal conductivity of 30 ppm/K and large CTE of 38 ppm/K, cause poor performance for conventional hBN-based composites in which the fillers are randomly oriented (Figure 1).[6] Therefore, controlling the orientation of hBN in the polymer matrix is critically important for optimizing the performance of its composites.

Magnetic alignment requires the filler to respond to the external magnetic field. Although hBN is not an intrinsically magnetic material, magnetically responsive hBN (mhBN) can be prepared from commercial hBN by surface modification using superparamagnetic iron oxide nanoparticles. The attachment of iron oxide nanoparticles to hBN surface is through the electrostatic interaction between the positively charged iron oxide nanoparticles and negatively charged hBN platelets. The mhBN platelets can orient themselves along the direction of external magnetic field to minimize the magnetic energy.[28] The size of the hBN platelet affects the strength of magnetic field required for efficient alignment. Using an optimized size reported by Erb et al., the mhBN platelet can be easily aligned using a rare-earth magnet.[28] As a result, the mhBN−epoxy composites inherit the anisotropic properties from the mhBN fillers. This process has been schematically illustrated in Figure 1.

2. EXPERIMENTAL SECTION

2.1. Materials. Hexagonal boron nitride (AC6041) was provided by Momentive, which has an averaged particle size of 5 μm and BET surface area of 6.77 m^2/g. The magnetic iron oxide nanoparticles solution (3.9 vol%) were supplied by Ferrotec (EMG 605) with the saturation magnetization of 22 mT and initial magnetic susceptibility of 3.02. The epoxy resin is the mixture of diglycidyl ether of bispenol A and 3,4-epoxy cyclohexylmethyl-3,4-epoxy cyclohexyl carboxylate. Hexahydro-4-methyl phthalic anhydride and 1-cyanoethyl-2-ethyl-4-methylimidazole were used as curing agent and catalyst respectively. Other chemicals were used as received.

2.2. Magnetic Modification of hBN. In a typical process, 4 g hBN powder was dispersed in water by gentle stir and sonication. 400 μL ferrofluid was then added and mixed by stirring. The suspension was incubated overnight to allow the bonding between hBN and iron oxide nanoparticles. After that, mhBN powder was separated from the suspension by centrifuge at 2000 rpm for 30 min and was dried at 60 °C in vacuum.

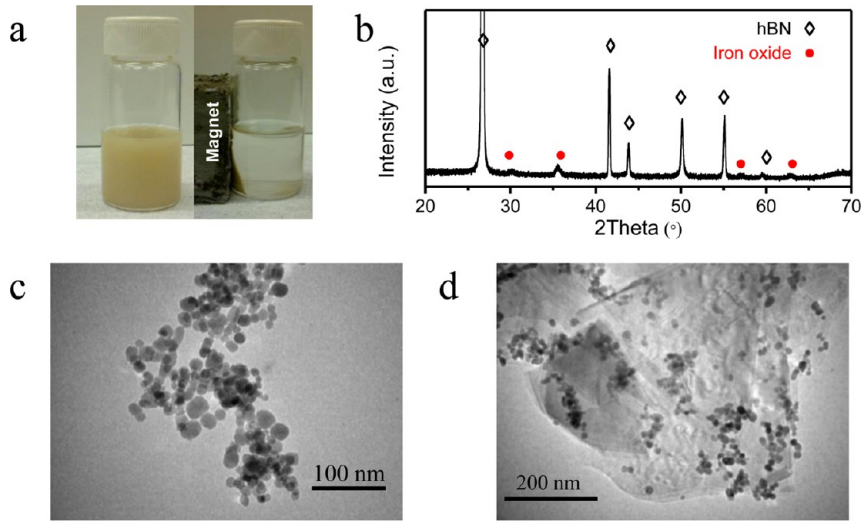

Figure 2. (a) Images of mhBN dispersion in acetone and its response to external magnetic field when a magnet is placed near the dispersion. (b) XRD pattern of mhBN; the black labels refer to peaks from hBN, and the red labels refer peaks from iron oxide nanoparticles. TEM images of (c) iron oxide nanoparticles and (d) mhBN.

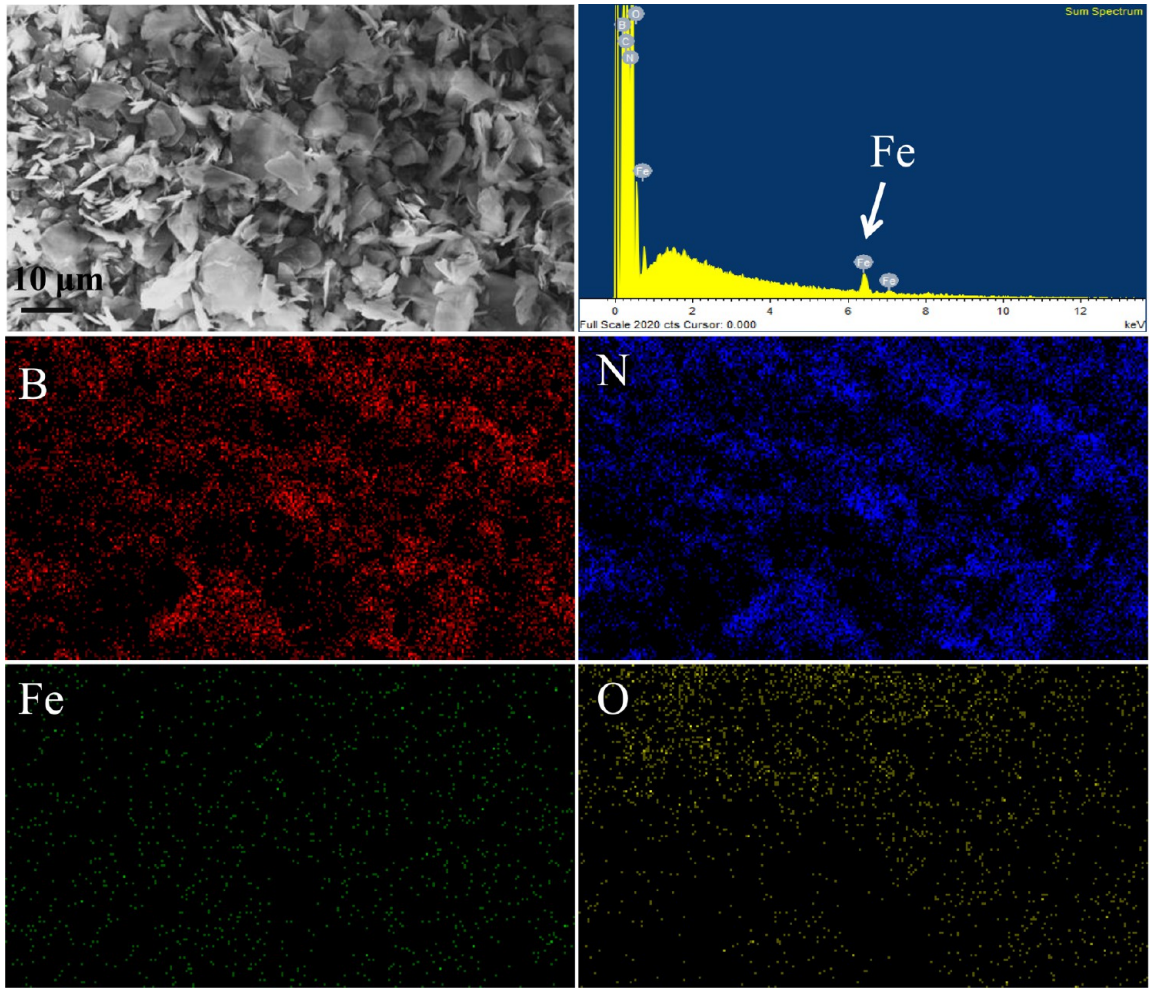

Figure 3. SEM image of mhBN and the EDS and elemental mapping collected from the same location.

2.3. Preparation of Aligned mhBN–Epoxy Composites. mhBN powder was mixed with epoxy resin by 5 min sonication. A small amount of acetone was added in this process to help the dispersion of mhBN and was then removed by vacuum at elevated temperatures. After that, the curing agent and catalyst were added and mixed by stirring. The composite was transferred to a Teflon mold and placed between two parallel arranged rare-earth magnets, as shown in Figure S1, Supporting Information. The strength of magnetic field is 400 mT measured by a Gaussmeter (Lakesure, model 410-SCT). The curing of epoxy was carried out by placing the whole fixture in an oven,

dx.doi.org/10.1021/am401939z | ACS Appl. Mater. Interfaces 2013, 5, 7633–7640

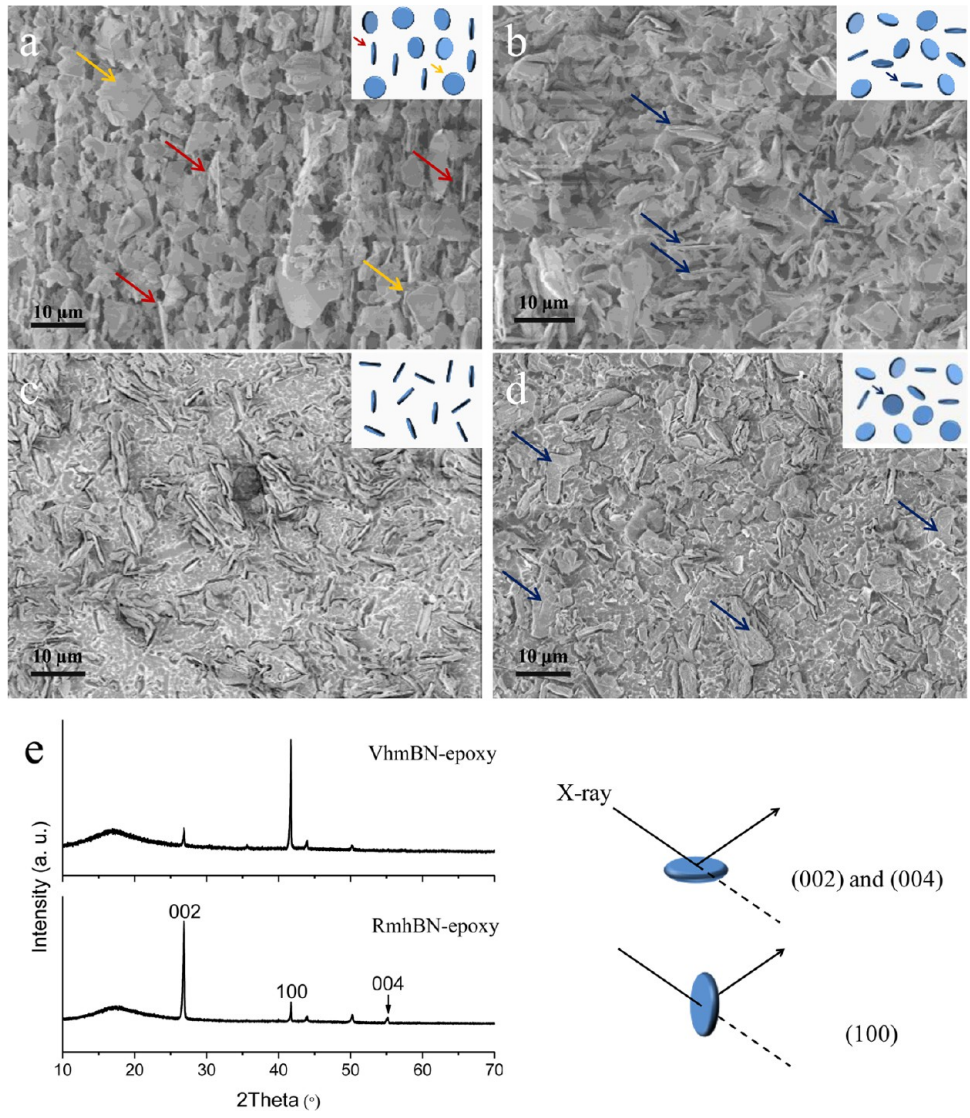

Figure 4. SEM cross-section images of RIE-treated 20 wt % (a) VmhBN−epoxy and (b) RmhBN−epoxy composites. Arrows point to the representative orientations; red and orange arrows indicate vertical alignment while blue arrows indicate horizontal alignment. Top-view images of RIE-treated 20 wt % (c) VmhBN−epoxy and (d) RmhBN−epoxy composites. Insets in these images schematically show the oriented fillers. (e) XRD patterns of VhmBN−epoxy and RhmBN−epoxy composites and the illustration of filler alignment effect on XRD pattern: the horizontally oriented mhBN is responsive for hBN (002) and (004) peaks and some vertically oriented mhBN are related to the (100) peak.

including both Teflon mold and the magnet, so that the magnetic field was applied throughout the curing process. The curing profile was 100 °C for 12 h and 150 °C for 1 h.

2.4. Characterizations. X-ray diffraction (XRD) analysis of mhBN and mhBN−epoxy composites was carried out with an X'Pert PRO Alpha-1 system using Cu Kα radiation (45 kV and 40 mA). The ζ-potential of iron oxide nanoparticles was measured using Malvern Zetasizer Nano ZS. Transmission electron microscopy (TEM) was carried out using the JEOL TEM 100CX. Scanning electron microscopy (SEM, LEO 1530 and 1550) was used to characterize the morphology of mhBN−epoxy composite surfaces using an accelerating voltage of 4 kV; samples were sputter coated with a thin layer of gold for better imaging. The energy dispersive spectroscopy was measured on uncoated mhBN powders using SEM 1530 equipped with an energy dispersive spectroscopy (EDS) detector. In order to observe the orientation of mhBN in the composite, the cracked composite surface was exposed to oxygen reaction ion etching (RIE) to etch away the outer epoxy layer. The Young's modulus of neat epoxy and epoxy composite were measured by TriboIndenter (TI 900, Hysitron) using a 10 μm cono-spherical probe. Thermomechanical analyzer (TMA, Q-400 TA Instruments) was used to measure the CTE of composites. The thermal diffusivity (α) of mhBN−epoxy composites was measured by the laser flash method using a LFA 471 (Netzsch). The thermal conductivity was calculated by $\kappa = \alpha C_p \rho$, in which ρ and C_p are the density and heat capacity of mhBN−epoxy composite. The C_p was measured using differential scanning calorimetry (DSC, Q-600 TA Instruments). All thermal measurements were carried out at room temperature. The complex viscosity of uncured hBN−epoxy composites were measured using discovery hybrid rheometer-2 (HR2, TA Instruments).

3. RESULTS AND DISCUSSION

To prepare mhBN, hBN platelets were dispersed in water and a solution of iron oxide nanoparticle was then added. Iron oxide nanoparticles are coated by cationic surfactants and have a ζ-potential of 30 mV, indicating the positive surface charge. The dispersed hBN have negative surface charges and thus a strong electrostatic interaction with iron oxide nanoparticles.[28,35] After being added to the hBN suspension, these magnetic nanoparticles are quickly attached onto the hBN surface.

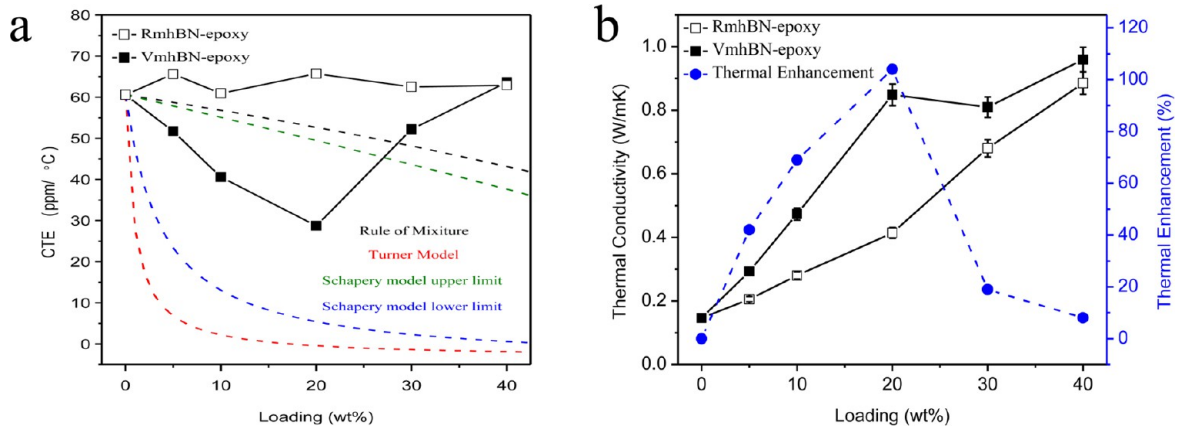

Figure 5. (a) Measured CTEs of VmhBN−epoxy and RmhBN−epoxy and the predicted CTEs by analytical models considering the anisotropic properties of hBN. (b) Thermal conductivity of VmhBN−epoxy and RmhBN−epoxy composites and corresponding thermal enhancement.

Consequently, the mhBN can respond to the external magnetic field as shown in Figure 2a. It is found that such electrostatic force is so strong that the magnetic response of mhBN is maintained after continuous sonication of the mhBN suspension. The presence of iron oxide particles is confirmed by the XRD pattern of mhBN (Figure 2b), in which feature peaks from both hBN and iron oxide are observed. The TEM characterization reveals that the size of iron oxide nanoparticles ranges from ∼10 to ∼25 nm (Figure 2c) and confirms the successful attachment of iron oxide nanoparticles to the surface of hBN platelets (Figure 2d). Further, the energy dispersive spectroscopy (EDS) analysis of mhBN reveals the presence of 0.32 at% iron (Figure 3). Moreover, the elemental mapping by EDS shows a uniform distribution of iron oxide, and no large agglomerate of nanoparticles is observed.

The mhBN−epoxy composites were prepared using a solvent transfer method, as described in the experimental section. During the curing of epoxy resin, an external magnetic field was applied by placing the mold between two magnets (Figure S1, Supporting Information), which guides the orientation of mhBN platelets in the composites. The amount of iron oxide nanoparticles on mhBN surface is an important factor affecting the magnetic alignment. We changed the loading of iron oxide nanoparticles on hBN from 0.5, 1, to 2 wt %. The 2 wt % loading is found to be maximum loading, which achieves the highest performance enhancement in terms of thermal conductivity. At 2 wt %, the magnetic susceptibility of mhBN is calculated to be 0.17 using the method developed by Erb et al.[28,36] The optimization of iron oxide loading is discussed in detail in Figure S2, Supporting Information. Moreover, the curing profile of composite was optimized to allow the efficient alignment of mhBN before the fully curing of epoxy resin, which is discussed in Figure S3, Supporting Information.

Vertical aligned mhBN−epoxy composites (VmhBN−epoxy) were prepared by applying a vertical magnetic field, and randomly oriented mhBN−epoxy composites (RmhBN−epoxy) were produced as control samples when no magnetic field was used. The SEM images of cracked surface of VmhBN−epoxy are shown in Figure S4, Supporting Information. The large roughness of the cracked surface of VmhBN−epoxy compared to that of neat epoxy indicates strong interfacial interactions between mhBN and epoxy resin. However, the orientation of mhBN platelets could not be visualized from SEM images due to the poor contrast between mhBN and epoxy resin, which are both electrically insulating. Therefore, oxygen reactive ion etching (RIE) was carried out to selectively remove the outer layer of epoxy resin, resulting in exposed the mhBN platelets. Parts a and b of Figure 4 show the SEM images of cracked cross-section of 20 wt % mhBN−epoxy composites after RIE treatment. It is clear that, in VmhBN−epoxy, the mhBN platelets are aligned along the direction of magnetic field so that the normal of platelets are perpendicular to the magnetic field direction and within the horizontal plane of the composite. In two representative cases, the aligned mhBN platelets are projected in the cross-section view as 1D vertical rods and 2D plates, which are indicated by red and orange arrows respectively. In contrast, in RmhBN−epoxy, the mhBN platelets are randomly orientated. One of most obvious indications is the existence of horizontally oriented platelets that are projected as 1D horizontal rods (indicated by blue arrows). To further prove the vertical alignment, the top-view SEM images of RIE-treated VmhBN−epoxy (Figure 4c) and RmhBN−epoxy (Figure 4d) were also collected. As expected, the mhBN platelets mostly show as 1D rods in VmhBN, whereas plate-shaped mhBN can be found in RmhBN. The observed SEM morphology is very close to the schematic drawings in the insets and clearly proves the effective magnetic alignment of mhBN in epoxy composites. Moreover, the magnetic alignment is with high uniformity as the SEM morphology of VmhBN−epoxy does not show any noticeable variation across the sample.

The XRD analysis of mhBN−epoxy composites in Figure 4e provides additional support for the magnetic alignment of mhBN. The hBN peaks in RmhBN−epoxy show similar intensities to those of mhBN powder, whereas dramatically changed peak intensities are observed in VmhBN−epoxy, suggesting the change of mhBN platelets orientations in the composite. Using the epoxy peak at ∼17° as a reference, the hBN (002) peak becomes six times weaker, the (004) peak disappears, and (100) peak becomes more than four times stronger in VmhBN−epoxy than those in RmhBN−epoxy. These changes in the XRD pattern of VmhBN−epoxy can be explained by the reduced amount of horizontally oriented mhBN and larger amount of vertically oriented mhBN, as schematically illustrated in Figure 4e.

The alignment of mhBN in its epoxy composite greatly impacts its CTEs due to aforementioned anisotropic properties of hBN. The linear CTEs of mhBN−epoxy composites were measured along their z direction. As shown in Figure 5a, the CTEs of RmhBN−epoxy at different loadings are in between

dx.doi.org/10.1021/am401939z | ACS Appl. Mater. Interfaces 2013, 5, 7633−7640

Table 1. Thermal Conductivity Enhancement ($\kappa_{composite}/\kappa_{resin}$) of Various BN−Polymer Composites

materials	filler size (μm)	loading (wt %)	thermal conductivity enhancement
hBN−epoxy[6]	12	20	∼3
	60−100	20	∼5.6
hBN−polyimide[10]	1 and 0.07	20	∼1.5
hBN−photosensitive polyimide[11]	0.07	20	∼1.5
hBN−polyimide[15]	0.7	∼40	∼6.8
hBN−epoxy (this work)	5	20	5.7 (VmhBN−epoxy) 2.8 (RmhBN−epoxy)

60 and 66 ppm/°C, close to the value for neat epoxy. In sharp contrast, VmhBN−epoxy shows a dramatic CTE reduction initially with the increase of filler loading, being as low as 28.7 ppm/°C at 20 wt %. However, further increase of filler loading above 20 wt % leads to larger CTEs than that of 20 wt % mhBN−epoxy. The less reduction of CTE at higher filler loading is because the alignment of mhBN requires low viscosity to allow the free rotation of mhBN platelets in epoxy resin. As the loading of mhBN increases above 20 wt %, the viscosity of mhBN−epoxy increases significantly (Figure S5, Supporting Information), which inhibits the filler alignment. Indeed, the examination of SEM cross-section images of 30 and 40 wt % VmhBN−epoxy reveals significant amount of unaligned mhBN platelets (Figure S6, Supporting Information), which do not appear in VmhBN−epoxy composites at lower loadings.

To better understand the CTE reduction effect by filler alignment, several analytical models are used to predict the CTE of VmhBN−epoxy considering the anisotropic properties of hBN (Supporting Information). The results are compared with the experimental values in Figure 5a. The simple rule of mixture assumes a uniform stress distribution in the composite and only account for the effect of the CTEs of filler and matrix. However, it fails to explain low CTE values, suggesting that the negative in-plane CTE of hBN is not the sole reason for the dramatic CTE reduction. Turner model assumes a homogeneous strain in the composite and gives an overestimated CTE reduction, indicating the critical role of high in-plane modulus of hBN for CTE reduction.[37] The Schapery model considers both normal and shear stresses between fillers and matrix and gives the upper and lower limits for CTEs.[38] The experimental CTEs of VmhBN−epoxy composites lie within the Schapery limits, showing that the negative in-plane CTE, high bulk modulus, and shear modulus of hBN all contribute to the CTE reduction of composites. These results also suggest that the large out-of-plane CTE and low bulk modulus cause the insignificant CTE reduction in RmhBN−epoxy and other hBN−epoxy composites.

The thermal conductivity of mhBN−epoxy composites is greatly enhanced by filler alignment. Figure 5b shows the *z*-direction thermal conductivities of VmhBN−epoxy and RmhBN−epoxy and the corresponding thermal enhancement. Here, the thermal enhancement is defined as the percentage of thermal conductivity improvement by magnetic alignment of mhBN: $(\kappa_{VmhBN-epoxy} - \kappa_{RmhBN-epoxy})/(\kappa_{RmhBN-epoxy})$ (κ refers to thermal conductivity). It is found that the thermal enhancement increases initially with the filler loading, reaching 104% at 20 wt %, and drops rapidly to 19 and 8% at 30 and 40 wt % respectively. The drop of thermal enhancement at high filler loadings is due to the same reason in the discussion of CTEs; that is, the increased viscosity hinders the alignment of mhBN during curing. Remarkably, at the optimal filler loading of 20 wt %, the thermal conductivity of VmhBN−epoxy is 0.85 W/mK, which is 5.7 times of measured value for neat epoxy (0.15 W/mK) and twice that for conventional silica-filled underfills. Table 1 compares the thermal conductivity enhancement of VmhBN−epoxy with reported hBN−polymer composites. It is evident that thermal conductivity enhancement of VmhBN−epoxy (5.7 times) represents one of the highest for 20 wt % filler loading.[6,10,11,15] Table 1 also tells that the filler alignment is the major reason for the exciting result because the RmhBN−epoxy shows 2.8 times enhancement of thermal conductivity, which is comparable to 1.5−3 times from similar works.

We used a modified effective medium approximation (EMA) to analyze our experimental data.[39] This model takes into account the thermal conductivity of filler and matrix, filler geometry and orientation, and thermal boundary resistance (TBR), and it could give important insights into the fundamental parameters governing the thermal transport in mhBN−epoxy composites. First, we study a possible adverse effect of adding iron oxide nanoparticles on hBN surface in terms of TBR change. It is well accepted that TBR is a major factor determining the overall thermal conductivity of composite materials. We have experimentally observed that the thermal conductivities of RmhBN−epoxy composites are lower than those of hBN−epoxy composite (Figure S7a, Supporting Information), which is an indication of TBR change. The actual TBR for each composite is extracted by fitting the measured thermal conductivity to EMA equations (Figure S7b and Table S1, Supporting Information). When assuming a filler aspect ratio of 0.05, the TBR for hBN−epoxy is found to be 76×10^{-9} m^2K/W, which increases over four times to 388×10^{-9} m^2K/W for RmhBN−epoxy. Although the result of dramatically increased TBR is qualitative, it tells clearly that the additional iron oxide nanoparticles in mhBN, with a relatively low thermal conductivity of ∼6 W/mK,[40] hinders the thermal transport across the hBN−epoxy interface probably by reducing the contact area between the hBN−hBN and hBN−epoxy.

Despite of the large TBR, a high thermal conductivity is still achieved by magnetic alignment. The significance of controlling the filler aligned is shown in Figure S8, Supporting Information. VmhBN−epoxy theoretically gives higher thermal conductivity than RmhBN−epoxy, while the horizontally aligned composites have much suppressed thermal conductivities. The theoretical thermal enhancement increases with filler loading, which is consistent with the experimental data. This trend can be explained by the increasing contribution of thermal transport through hBN fillers at higher loadings. Moreover, it is interesting to note that the predicted thermal enhancement is lower than that observed in our experiments. For example, at 20 wt %, the predicted thermal enhancement is only ∼32%, compared to the experimental value of 104%. This disparity could attribute to the complexity of real systems such as the variation of mhBN size, shape, and thickness. Specifically, there

are several aspects that lead the EMA calculation to underestimate thermal conductivities for VmhBN–epoxy and overestimate those for RmhBN–epoxy. First, uniform TBR values are simply assumed in EMA calculation. However, in the case of VmhBN–epoxy, the TBR for the hBN edges–epoxy interface could be much smaller than that for hBN basal plane–epoxy interface. Such anisotropic TBR has been found in materials with similar atomic structure to hBN, such as graphite and carbon nanotubes.[41−44] Tentative fitting of the thermal conductivities of VmhBN–epoxy to EMA equation indeed shows a 1 order of magnitude smaller TBR (Figure S9, Supporting Information). Second, the assumed isotropic thermal conductivity for hBN (600 W/mK) overestimates the thermal conductivity of RmhBN–epoxy as the out-of-plane thermal conductivity of hBN is considerably smaller (30 W/mK). Third, the gravity force tends to horizontally orientate the mhBN platelets and lowers the thermal conductivities. Thus, a complete random orientation assumed in modeling overestimates the thermal conductivity for RmhBN–epoxy.

The mechanical and dielectric properties of polymer composite are also important for electronic packaging applications. As shown in Figure 6, the Young's modulus of neat epoxy and 20 wt % RmhBN–epoxy are 2.70 and 3.45 GPa, respectively. A clear anisotropicity is observed for 20 wt % VmhBN–epoxy with a higher *z*-direction modulus of 4.55 GPa and a lower *x*–*y* direction modulus of 3.52 GPa, which results from the magnetic alignment and high in-plane modulus of hBN. Moreover, dielectric constant and dielectric loss tangent of 20 wt % VmhBN–epoxy only shows slight increase from those of neat epoxy (Figure S10, Supporting Information). This result could be attributed to the low dielectric constant and high electric resistivity of hBN fillers and is highly desirable for underfill applications.

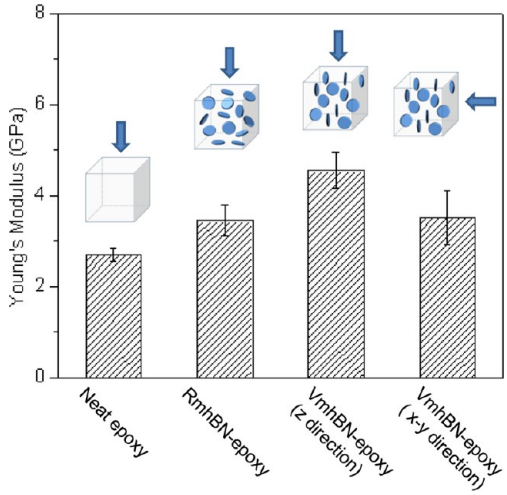

Figure 6. Young's modulus of neat epoxy, 20 wt % RmhBN–epoxy and VmhBN–epoxy along *z* direction and in *x*–*y* direction (arrows indicate the measurement direction).

The VmhBN–epoxy is a promising material for electronic encapsulation where low CTE and high thermal conductivity are required to meet the increasingly stringent device reliability and thermal management needs. We used finite-element analysis (FEA) to investigate the application of VmhBN–epoxy as an underfill from a thermomechanical point of view. The underfill is an encapsulation material widely used to improve the reliability of solder interconnects. Figure 7a shows a schematic of a flipped IC assembled on an organic substrate with solder bumps that are encapsulated with an underfill. Tables S2 and S3 in the Supporting Information provide the dimensions of one such assembly and related material properties. To compare the performance of VmhBN–epoxy and RmhBN–epoxy, a three-dimensional half-symmetric generalized plane deformation (GPD) model of the assembly was created, and the model was simulated to be thermally cycled between 0 and 100 °C. It is known that the corner solder joints experience the highest thermo-mechanical stress/strains due to coefficient of CTE mismatch between silicon die and organic substrate. The fatigue life of corner solder joints can be determined using the accumulated plastic strain as a damage metric in a Coffin–Manson type relationship.[45] As seen in Figure 7b, the results from the simulation show that VmhBN–epoxy has a smaller accumulated plastic strain than RmhBN–epoxy; this is attributed to the lower *z*-direction CTE of VmhBN–epoxy compared to that of RmhBN–epoxy. Thus, the predicted solder fatigue life is 2014 cycles for VmhBN–epoxy and 1769 cycles for RmhBN–epoxy. This value is beyond the typical industrial requirements for commercial packages.

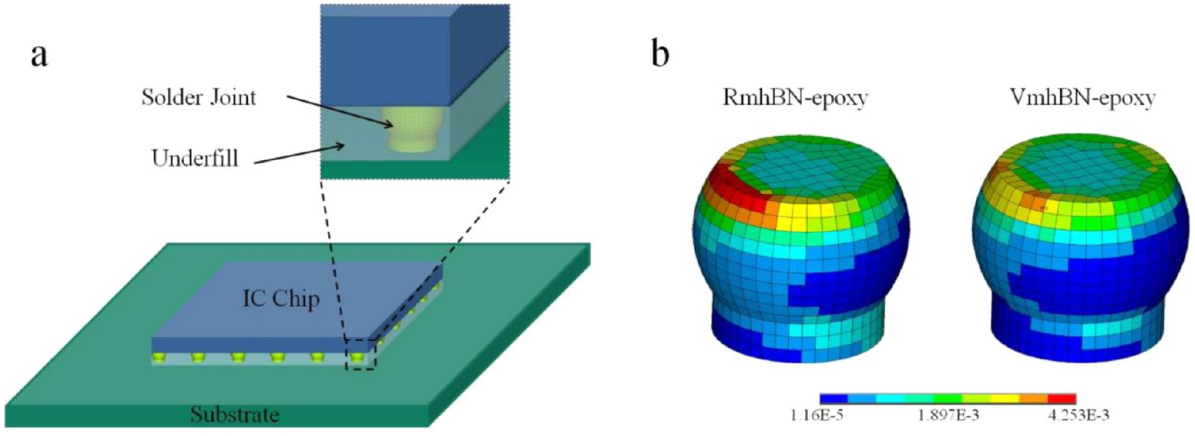

Figure 7. FEA of VmhBN–epoxy as a potential underfill in a flip-chip package. (a) Schematic illustration of the structure of flip-chip packaging used for FEM. The solder joint interconnections between the substrate and IC chip are encapsulated by underfill for reliability improvement. (b) The accumulated plastic stain of a peripheral solder joint when RmhBN–epoxy or VmhBN–epoxy is used as underfills.

4. CONCLUSION

In summary, we modified the hBN with magnetic iron oxide nanoparticles and demonstrated controlled alignment of mhBN in epoxy composite by an external magnetic field. The resulting mhBN−epoxy composite inherits anisotropic properties from the hBN fillers. Remarkably, low CTE and high thermal conductivity along the alignment direction have been achieved at low filler loadings so that the excellent processablity and mechanical and dielectric properties of epoxy resin can be maintained in these composites. To the best of our knowledge, this is the first exploration on the alignment of hBN in polymer composites and its impact to materials properties. The anisotropic polymer composite, which can be prepared using a fairly low-cost method, has very promising applications as underfills or TIMs for advanced microelectronics packaging.

■ ASSOCIATED CONTENT

Supporting Information

Setup for magnetic alignment; SEM images of VmhBN−epoxy and RmhBN−epoxy; rheological measurements; theoretical models for CTE and thermal conductivity calculation. FEA analysis of VmhBN−epoxy for underfill applications. This information is available free of charge via the Internet at http://pubs.acs.org/.

■ AUTHOR INFORMATION

Corresponding Author

*Phone: (404) 894-8391. Fax: (404) 894-9140. E-mail: cp.wong@mse.gatech.edu.

Notes

The authors declare no competing financial interest.

■ ACKNOWLEDGMENTS

The authors would like to thank Mr. Xi Liu and Mr. Nicholas Ginga for their help on triboindenter measurements, Ms. Vanessa Rene from Ferrotec (U.S.A.) for providing iron oxide nanoparticles, and Mr. Jeffrey Shinko from Momentive for supplying the hBN powders.

■ REFERENCES

(1) Garimella, S. V.; Fleischer, A. S.; Murthy, J. Y.; Keshavarzi, A.; Prasher, R.; Patel, C.; Bhavnani, S. H.; Venkatasubramanian, R.; Mahajan, R.; Joshi, Y.; Sammakia, B.; Myers, B. A.; Chorosinski, L.; Baelmans, M.; Sathyamurthy, P.; Raad, P. E. *IEEE Trans.Compon. Packag. Technol.* **2008**, *31*, 801−815.
(2) Wong, C. P.; Moon, K. S.; Li, Y. *Nano-Bio-Electronic, Photonic and MEMS Packaging*; Springer: New York, 2010; p 277−314.
(3) Lu, D.; Wong, C. P. *Materials for Advanced Packaging*; Springer: New York, 2009.
(4) Prasher, R. *Proc. IEEE* **2006**, *94*, 1571−1586.
(5) Wong, C. P.; Bollampally, R. S. *J. Appl. Polym. Sci.* **1999**, *74*, 3396−3403.
(6) Liang, Q. Z.; Xiu, Y. H.; Lin, W.; Moon, K. S.; Wong, C. P. *Proc. Electron. Compon. Technol. Conf.* **2009**, 437−440.
(7) Sun, Y. Y.; Zhang, Z. Q.; Wong, C. P. *J. Colloid Interface Sci.* **2005**, *292*, 436−444.
(8) Sun, Y. Y.; Zhang, Z. Q.; Wong, C. P. *IEEE Trans. Compon. Packag. Technol.* **2006**, *29*, 190−197.
(9) Song, W. L.; Wang, P.; Cao, L.; Anderson, A.; Meziani, M. J.; Farr, A. J.; Sun, Y. P. *Angew. Chem., Int. Ed.* **2012**, *51*, 6498−6501.
(10) Li, T. L.; Hsu, S. L. C. *J. Phys. Chem. B* **2010**, *114*, 6825−6829.
(11) Li, T. L.; Hsu, S. L. C. *J. Appl. Polym. Sci.* **2011**, *121*, 916−922.
(12) Lin, Z. Y.; Yao, Y. G.; Mcnamara, A.; Moon, K. S.; Wong, C. P. *Proc. Electron. Compon. Technol. Conf.* **2012**, 1437−1441.
(13) Zhang, R. W.; Lin, W.; Moon, K. S.; Wong, C. P. *ACS Appl. Mater. Interfaces* **2010**, *2*, 2637−2645.
(14) Shahil, K. M. F.; Balandin, A. A. *Nano Lett.* **2012**, *12*, 861−867.
(15) Sato, K.; Horibe, H.; Shirai, T.; Hotta, Y.; Nakano, H.; Nagai, H.; Mitsuishi, K.; Watari, K. *J. Mater. Chem.* **2010**, *20*, 2749−2752.
(16) Marconnett, A. M.; Yamamoto, N.; Panzer, M. A.; Wardle, B. L.; Goodson, K. E. *ACS Nano* **2011**, *5*, 4818−4825.
(17) Li, L.; Yang, Z. B.; Gao, H. J.; Zhang, H.; Ren, J.; Sun, X. M.; Chen, T.; Kia, H. C.; Peng, H. S. *Adv. Mater.* **2011**, *23*, 3730−3735.
(18) Lin, W.; Moon, K. S.; Wong, C. P. *Adv. Mater.* **2009**, *21*, 2421−2424.
(19) Wei, C.; Dai, L. M.; Roy, A.; Tolle, T. B. *J. Am. Chem. Soc.* **2006**, *128*, 1412−1413.
(20) Lanticse, L. J.; Tanabe, Y.; Matsui, K.; Kaburagi, Y.; Suda, K.; Hoteida, M.; Endo, M.; Yasuda, E. *Carbon* **2006**, *44*, 3078−3086.
(21) Terao, T.; Zhi, C. Y.; Bando, Y.; Mitome, M.; Tang, C. C.; Golberg, D. *J. Phys. Chem. C* **2010**, *114*, 4340−4344.
(22) Cooper, C. A.; Ravich, D.; Lips, D.; Mayer, J.; Wagner, H. D. *Compos. Sci. Technol.* **2002**, *62*, 1105−1112.
(23) Jin, L.; Bower, C.; Zhou, O. *Appl. Phys. Lett.* **1998**, *73*, 1197−1199.
(24) Haggenmueller, R.; Gommans, H. H.; Rinzler, A. G.; Fischer, J. E.; Winey, K. I. *Chem. Phys. Lett.* **2000**, *330*, 219−225.
(25) Yousefi, N.; Gudarzi, M. M.; Zheng, Q. B.; Aboutalebi, S. H.; Sharif, F.; Kim, J. K. *J. Mater. Chem.* **2012**, *22*, 12709−12717.
(26) Liang, Q. Z.; Yao, X. X.; Wang, W.; Liu, Y.; Wong, C. P. *ACS Nano* **2011**, *5*, 2392−2401.
(27) Correa-Duarte, M. A.; Grzelczak, M.; Salgueirino-Maceira, V.; Giersig, M.; Liz-Marzan, L. M.; Farle, M.; Sierazdki, K.; Diaz, R. *J. Phys. Chem. B* **2005**, *109*, 19060−19063.
(28) Erb, R. M.; Libanori, R.; Rothfuchs, N.; Studart, A. R. *Science* **2012**, *335*, 199−204.
(29) Goubault, C.; Jop, P.; Fermigier, M.; Baudry, J.; Bertrand, E.; Bibette, J. *Phys. Rev. Lett.* **2003**, *91*, 260802.
(30) Singh, H.; Laibinis, P. E.; Hatton, T. A. *Nano Lett.* **2005**, *5*, 2149−2154.
(31) Ge, J. P.; Hu, Y. X.; Yin, Y. D. *Angew. Chem., Int. Ed.* **2007**, *46*, 7428−7431.
(32) Lee, D.; Cohen, R. E.; Rubner, M. F. *Langmuir* **2007**, *23*, 123−129.
(33) Fresnais, J.; Berret, J. F.; Frka-Petesic, B.; Sandre, O.; Perzynski, R. *Adv. Mater.* **2008**, *20*, 3877−3881.
(34) Yan, M.; Fresnais, J.; Sekar, S.; Chapel, J. P.; Berret, J. F. *ACS Appl. Mater. Interfaces* **2011**, *3*, 1049−1054.
(35) Crimp, M. J.; Oppermann, D. A.; Krehbiel, K. *J. Mater. Sci.* **1999**, *34*, 2621−2625.
(36) Erb, R. M.; Son, H. S.; Samanta, B.; Rotello, V. M.; Yellen, B. B. *Nature* **2009**, *457*, 999−1002.
(37) Turner, P. S. *J. Res. Natl. Bur. Stand.* **1946**, *37*, 239−250.
(38) Schapery, R. A. *J. Compos. Mater.* **1968**, *2*, 380−404.
(39) Nan, C. W.; Birringer, R.; Clarke, D. R.; Gleiter, H. *J. Appl. Phys.* **1997**, *81*, 6692−6699.
(40) Slack, G. A. *Phys. Rev.* **1962**, *126*, 427−441.
(41) Hirotani, J.; Ikuta, T.; Nishiyama, T.; Takahashi, K. *Nanotechnology* **2011**, *22*, 315702.
(42) Prasher, R. *Phys. Rev. B* **2008**, *77*, 075424.
(43) Duda, J. C.; Hopkins, P. E.; Beechem, T. E.; Smoyer, J. L.; Norris, P. M. *Superlattices Microstruct.* **2010**, *47*, 550−555.
(44) Schmidt, A. J.; Collins, K. C.; Minnich, A. J.; Chen, G. *J. Appl. Phys.* **2010**, *107*, 104907.
(45) Pang, J. H. L.; Xiong, B. S.; Low, T. H. *Thin Solid Films* **2004**, *462*, 408−412.